Molecular Detection of SARS-Cov-2 in Exhaled Breath Using a Portable Sampler

Tim Stakenborg
imec
Joren Raymenants
KU Leuven https://orcid.org/0000-0001-6441-1843
Ahmed Taher
imec
Elisabeth Marchal
imec
Bert Verbruggen
imec
Sophie Roth
imec
Ben Jones
imec
Abdul Yurt
imec
Wout Duthoo
imec
Klaas Bombeke
imec / UGent
Maarten Fauvart
imec
Julien Verplanken
imec
Rodrigo Wiederkehr
imec
Aurelie Humbert
imec
Chi Dang
imec
Evi Vlassaks
imec
Alejandra Jauregui Uribe

imec
Zhenxiang Luo
imec
Chengxun Liu
imec
Kirill Zinoviev
imec
Riet Labie
imec
Aduén Darriba Frederiks
UGent
Jelle Saldien
imec UGent
Kris Covens
imec
Pieter Berden
imec
Bert Schreurs
VUB
Joost Van Duppen
imec
Rabea Hanifa
imec
Megane Beuscart
imec
Van Pham
imec
Erik Emmen
imec
Annelien Dewagtere
imec
Ziduo Lin
imec
Marco Peca
imec
Youssef El Jerrari
imec
Chinmay Nawghane
imec

Chad Arnett
imec
Andy Lambrechts
imec
Paru Deshpande
imec
Katrien Lagrou
KU Leuven
Paul De Munter
KU Leuven
Emmanuel André
KU Leuven
Nik Van den Wijngaert (nik.vandenwijngaert@imec.be)
imec
Peter Peumans
imec

Article

Keywords:

Posted Date: December 20th, 2021

DOI: https://doi.org/10.21203/rs.3.rs-1104361/v1

MOLECULAR DETECTION OF SARS-COV-2 IN EXHALED BREATH USING A PORTABLE SAMPLER

Tim Stakenborg[1], Joren Raymenants[7,9], Ahmed Taher[1], Elisabeth Marchal[1], Bert Verbruggen[2], Sophie Roth[1], Ben Jones[1], Abdul Yurt[2], Wout Duthoo[3], Klaas Bombeke[4], Maarten Fauvart[1], Julien Verplanken[3], Rodrigo S. Wiederkehr[1], Aurelie Humbert[1], Chi Dang[1], Evi Vlassaks[2], Alejandra L. Jáuregui Uribe[1], Zhenxiang Luo[2], Chengxun Liu[1], Kirill Zinoviev[1], Riet Labie[2], Aduen Darriba Frederiks[5], Jelle Saldien[5], Kris Covens[1], Pieter Berden[1,10], Bert Schreurs[6], Joost Van Duppen[1], Rabea Hanifa[1], Megane Beuscart[1], Van Pham[1], Erik Emmen[2], Annelien Dewagtere[1], Ziduo Lin[2], Marco Peca[1], Youssef El Jerrari[1], Chinmay Nawghane[2], Chad Arnett[2], Andy Lambrechts[2], Paru Deshpande[1], Katrien Lagrou[7,8], Paul De Munter[7,9], Emmanuel André[7,8], Nik Van den Wijngaert[2, ✉], Peter Peumans[1]

[1] *Life Science Technologies department, imec, Kapeldreef 75, 3001 Leuven, Belgium*

[2] *Imec Solutions department, imec, Kapeldreef 75, 3001 Leuven, Belgium*

[3] *Enabling Digital Transformations department, imec, 9000 Ghent, Belgium*

[4] *imec-mict-UGent, Department of Communication Sciences, Ghent University, Platteberg 11, 9000 Gent, Belgium*

[5] *imec-mict-UGent, Department of Industrial Systems Engineering and Product Design, Ghent University, Platteberg 11, 9000 Gent, Belgium*

[6] *Department of Business, Research Group Management and Strategy, Vrije Universiteit Brussel, Pleinlaan 2, 1050 Brussels, Belgium.*

[7] *Department of Microbiology, Immunology and Transplantation, KU Leuven, Herestraat 49, 3000 Leuven, Belgium*

[8] *Department of laboratory medicine, University Hospitals Leuven, Herestraat 49, 3000 Leuven, Belgium*

[9] *Department of general internal medicine, University Hospitals Leuven, Herestraat 49, 3000 Leuven, Belgium*

[10] *Department of Physics and Astronomy, KU Leuven, Celestijnenlaan 200D, 3001, Leuven, Belgium*

Corresponding author: Nik Van den Wijngaert, imec, Kapeldreef 75, 3001 Heverlee, Belgium. Mail: Nik.VandenWijngaert@imec.be

Contributions:

TS, AY, AL, PD, NVDW, PP all contributed to the general concept, daily follow-up and project management. EM, MF, KC, PB, JVD, RH, MB, VP worked on the PCR assay development and testing. KB, WD, ADF, JS designed and performed the breathing tests with healthy volunteers. RL, EE, CA, CN designed the clamp and contributed to the breath sampler. SR, YEJ, MP, RW, CL characterized the sieve and clamp. AT, BJ designed and simulated the silicon sieves. EV, BV, JR, KL, PDM, EA designed and supervised the clinical studies. AH, CD ensured the silicon sieve processing. AU, KZ, AD, ZL worked on the development of the portable PCR instrument. BS, JV, ZL performed data analysis.

ABSTRACT

The SARS-CoV-2 pandemic has highlighted the need for improved technologies to help control the spread of contagious pathogens. While rapid point-of-need testing plays a key role in strategies to rapidly identify and isolate infectious patients, a cornerstone for any disease-control strategy, current test approaches have significant shortcomings related to assay limitations and sample type. Direct quantification of viral shedding in exhaled particles may offer a better rapid testing approach, since SARS-CoV-2 is believed to spread mainly by aerosols. It potentially measures contagiousness directly, the sample is easy to obtain, its production can be standardized between patients, and the limited sample volume lends itself to a fast and sensitive analysis. In view of these benefits, we developed and tested an approach where exhaled particles are efficiently sampled using inertial impaction in a micromachined silicon chip, followed by an in-situ RT-qPCR molecular assay to detect SARS-CoV-2 shedding. We demonstrate that sampling subjects using a one-minute breathing protocol, yields sufficient viral RNA to detect infections with a sensitivity comparable to standard sampling methods. A longitudinal study revealed clear differences in the temporal dynamics of viral load for nasopharyngeal swab, saliva, breath, and antigen tests. Overall, after an infection, the breath-based test is the first to consistently report a negative result, putatively signaling the end of contagiousness and further emphasizing the potential of this tool to help manage the spread of airborne respiratory infections.

MAIN

Person-to-person transmission facilitated by respiratory droplets plays an important role in the spreading of infectious diseases. For SARS-CoV-2, airborne transmission is thought to occur over both short and long distances by a continuum of exhaled particle sizes. While large droplets settle quickly, smaller particles can remain aloft for hours and travel long distances[1,2]. Especially in poorly ventilated spaces where people congregate, exhaled particles potentially containing infectious virus particles can accumulate, leading to a significantly increased infection risk[3]. While transmission through aerosols is difficult to demonstrate directly, multiple studies have identified airborne SARS-CoV-2 to be viable[4,5] and reports of super-spreader events point to exhaled particles playing a key role in viral spreading[6]. Rapid diagnosis and contact tracing together with quarantining of potentially infected persons has proven to be a cornerstone of public health measures deployed by many countries to contain spread in the absence of immunity[7]. While nasopharyngeal swab tests are the most common method of sampling[8], it is perceived as unpleasant by most subjects[9] and only indicates if a person has been infected recently. Given the clear role of exhaled particles in the transmission of SARS-CoV-2, there is need for techniques to analyse a person's contagiousness at the point-of-need. Such a test would constitute a major breakthrough for the containment of SARS-CoV-2 and other respiratory pathogens[10]. In view of these needs, we have developed a portable breath sampler capable of collecting respiratory particles in combination with a standard molecular test as a non-invasive method for routine sampling and to yield insight into a person's contagiousness (see Fig. 1).

Fig. 1: Schematic overview of the portable device to sample exhaled particles.

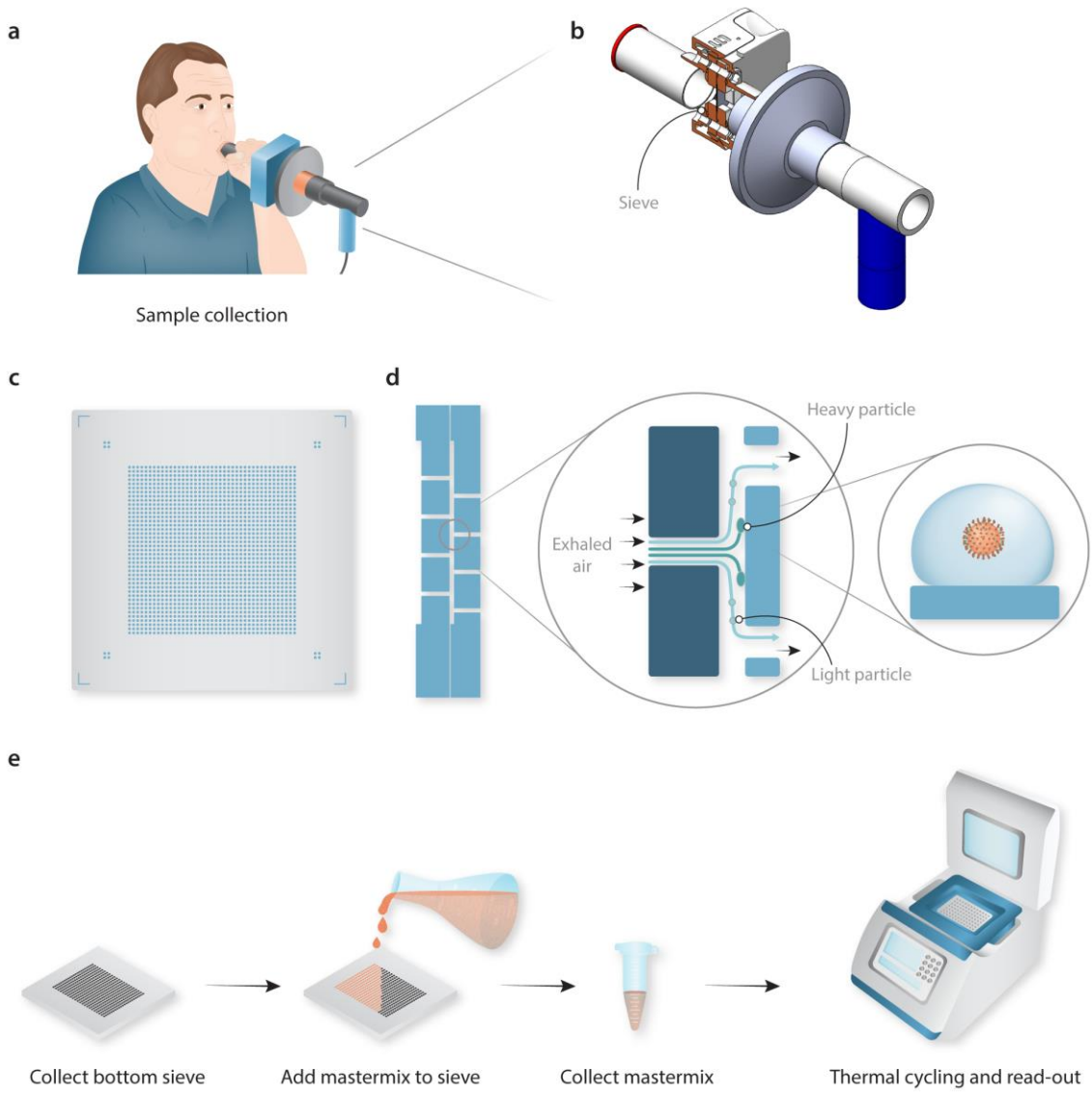

a, Schematic representation of a person breathing into the sampling device. **b**, Design of the disposable sampling device with the position of the silicon sieve indicated and kept in place by a holder consisting of an aluminium pre-heated block with O-rings for sealing. A mouthpiece is used in front, and a viral filter in between the silicon impactor and a spirometer (indicated in blue) for measuring flow rate during sampling. **c**, Schematic top-view of the final sieve, 22x22 mm^2 in size, consisting of an array of 1600 nozzles with a diameter of 150 µm. **d**, The non-integrated, non-monolithic impactor consists of two sieves stacked on top of each other, creating a gap of 30µm between the two arrays of holes (the single piece, monolithic impactor is described in Fig. 4). Exhaled particles, some containing virus, are collected on the bottom sieve by inertial impaction, while air and very small particles (<300 nm) are directed to the outlet nozzles and exit without

impacting. **e**, Schematic overview of the used protocol for this non-monolithic version of the impactor. The bottom sieve is removed from the sample device and master mix is pipetted on top followed by a brief spin to collect the sample. The sample is transferred to a 96-well plate and a RT-qPCR is conducted using a commercial thermal cycler.

IMPACTOR DESIGN AND PARTICLE CAPTURE EFFICIENCY

Various techniques have been used to collect airborne viral particles, including large liquid impingers, solid impactors and electrostatic precipitators[11]. These approaches are, however, limited due to their excessive size or large pressure drop that is required for efficient particle collections. Portable solutions to collect exhaled viral particles, relying on sampling the exhaled breath condensate[12] or using filter papers[13], allow little design flexibility and need significant sample volumes for analysis. A recent study that used face mask filters yielded a subpar sensitivity[14]. To efficiently capture exhaled particles from breath while minimizing perceived effort and resulting sample volume, a silicon impactor was designed (see Fig. 1c-d). The dimensions and performance attributes of the impactor chip were determined by numerical simulations (see Fig. 2a-b). As the relationship between flow rate, pressure drop, and collection efficiency needs to be balanced carefully; the design requirement was to efficiently capture particles as small as 300 nm-diameter at a flow rate of 0.6 L/sec and with a pressure drop of less than 30 mbar, while keeping the chip area to a minimum. The pressure drop was chosen to ensure most people felt comfortable while exhaling through the sieve, which was confirmed based on results of a mixed test panel (see Fig. 2b). Results of the same test panel showed that a higher pressure drop – especially in combination with a low achieved flow rate – resulted in a less comfortable user experience (see Fig. 2b). The measured pressure drop and the collection efficiency of the silicon impactor matched simulation results (see Fig. 2b-c). Consistent capture efficiencies over 85% were measured for particles larger than 300 nm diameter at a flow rate of 0.6 L/s.

While larger particles are more easily diverted from the air flow, the collection of smaller particles requires a higher flow rate with an associated pressure drop through the nozzles.

Fig. 2: Non-monolithic silicon impactor characteristics.

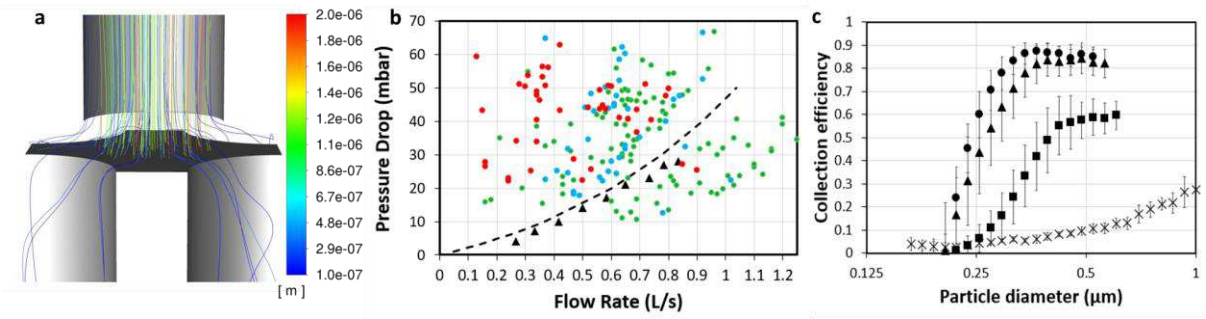

a, Fluidic simulation for the designed sieve visualizing particle trajectories of different sizes, coloured by particle diameter, generated using Ansys Fluent software for a nozzle with a diameter of 150 µm at a flow rate of 0.6 L/s. **b**, Experimentally (triangles) measured and simulated (dotted line) pressure drop of the sieve versus flow rate. The rated comfort levels of a test panel for different flow rates and pressure drops are indicated as well with green dots being perceived as a comfortable, blue as a neutral and red as an uncomfortable user experience. **c**, Normalized capture efficiency of the impactor as a function of particle diameter for different flow rates (crosses: 0.08 L/s, rectangles: 0.25 L/s, triangles: 0.42 L/s, and circles: 0.6 L/s). The error bars correspond to the standard deviation over 4 different impactor chips.

SARS-CoV-2 DETECTION IN EXHALED PARTICLES

To demonstrate the efficient detection of SARS-CoV-2 in exhaled breath using the silicon impactors, a first clinical study was performed focussing on sampling patients that were hospitalized. Both SARS-CoV-2 positive (considered positive based on an earlier nasopharyngeal swab-sampled laboratory RT-qPCR test) and healthy volunteers (considered negative) were asked to perform 20 tidal exhalations into the portable breath sampler (Fig 1b). A nasopharyngeal swab sample was taken contemporaneously. Next, the impactor chips were retrieved from the sampler and rinsed with master mix to perform a direct RT-qPCR test (see Fig. 1e). The swabs were analysed with a reference RT-qPCR assay. Of the 55 subjects tested, 23 were negative using both nasopharyngeal swab and breath tests. Of the 32 patients determined positive using the nasopharyngeal swab, the breath sampling method confirmed presence of SARS-CoV-2 in 24 patients and 8 yielded a negative result (i.e. 75 % positive agreement and 100% negative agreement, see Supplementary Info). The threshold cycle (Ct) value of the breath samples tends to be higher than that of the nasopharyngeal samples, indicating that significantly less viral RNA is captured using breath sampling. However, for 4 subjects, three of which were asymptomatic, the breath sample had a lower Ct value compared to the nasopharyngeal swab (see Source Data 1). Three of these patients were retested 3 or 4 days later and consistently showed a positive breath test. These results corroborate earlier reports that infected persons without symptoms may shed more viral particles compared to some symptomatic patients[15].

To assess the impact of different breathing protocols on the sensitivity of the breath-based RT-qPCR test, a second clinical study was conducted in ambulatory patients comparing 2 and 4 minutes of tidal breathing, 10 forced exhalations, and 1 minute of vocalizing whilst

168 exhaling. In this trial, 56 subjects visiting a student COVID-19 test center[16] were sampled
169 with all four breathing protocols. A rapid antigen test was used to pre-screen these
170 participants. Of the 56 participants, 33 tested negative and 23 tested positive on a
171 nasopharyngeal swab laboratory RT-qPCR test which was used as a reference. Breath
172 sampling using vocalization was the most sensitive breath sampling protocol, yielding a
173 positive result in 17 out of 23 positive participants (i.e. 74 % positive agreement and 100%
174 negative agreement, see Supplementary Info). The better performance of vocalization may
175 be explained by a higher rate of emission of particles upon vocalizing as opposed to tidal
176 breathing[17,18]. The forced exhalation approach appeared much less sensitive (i.e. 22% positive
177 agreement) in this student group (average ~22 years old, ambulatory, upright position during
178 sampling) as compared to the first study on a cohort of hospitalized patients (average ~62
179 years old, in-patient, recumbent position during sampling), suggesting a possible effect of age,
180 sampling position, a lower respiratory tract infection prompting admission, or another
181 covariate not assessed within this study[19,20]. The observed difference in positive percentage
182 agreement between breathing techniques (22% vs 74%) is striking and warrants further
183 research. In both studies, the observed Ct values were reproducible (SD 0.94) all above 23
184 (below ~10^4 viral copies/sieve) and mostly above 27 (below ~10^3 copies/sieve), in the same
185 order of magnitude as earlier empirical data assessing concentrations of viral pathogens in
186 exhaled breath during 30 min of tidal breathing[21,22].
187

LONGITUDINAL STUDY

The superior sensitivity of molecular assays means they are better at detecting infections early as compared to rapid antigen tests[23]. However, they risk over-diagnosing active SARS-CoV-2 replication at the tail end of an infection[24]. Contact tracing studies show that SARS-CoV-2 transmission peaks early on in the infection, already starting few days prior to symptom onset and declining rapidly in the first week thereafter[25,26]. These results correspond to the rapid disappearance of infectious virus one week after it can be first detected[27–29]. Currently no rapid, scalable diagnostic test is able to discern contagiousness over the full course of an infection with SARS-CoV-2.

A longitudinal study was set up to assess how RT-qPCR on exhaled particles collected while vocalizing corresponds to RT-qPCR results using nasopharyngeal swabs and saliva samples, and to a rapid antigen test performed on nasopharyngeal swabs, during the course of a COVID-19 infection. High risk contacts of confirmed COVID-19-positive subjects were followed up prospectively to study infections from an early phase onwards (see methods section and extended data Fig. 7). Of the 58 high-risk contacts included in the study, 11 developed an infection.

In contrast to the moderate 74% positive agreement between the breath and nasopharyngeal tests in our in-patient study, the individual graphs of study participants in this ambulatory longitudinal study show very similar trends between quantitative results of RT-qPCR (Fig. 3). We find that RT-qPCR on exhaled particles turned positive in a similar timeframe as RT-qPCR on nasopharyngeal and saliva samples while the antigen test is less sensitive at the start of an infection. Quickly after the first positive test (day 2 onwards), a 100% positive agreement is observed between the nasopharyngeal and breath RT-qPCR up

to day 6. From day 7 onwards, the agreement drops as less exhaled virus particles were detected and more breath tests turned negative (see Extended Data Fig. 6). Exhaled particle-based viral loads appear to have an early peak value followed by a monotonic decline, in contrast to the other sample types (Fig. 3b). In general, we observe that the breath-based RT-qPCR becomes negative before the other molecular tests. These data suggest that RT-qPCR on breath appears to constitute a respiratory sample associated with viral kinetics which are distinct from other frequently used sample types. If these preliminary findings revealing high sensitivity in the initial infection phase, early peak value in viral concentration measured and more rapid return to negativity as opposed to other respiratory samples are confirmed, breath RT-qPCR is closer to a contagiousness test than current state-of-the-art tests are.

Fig. 3: Longitudinal study.

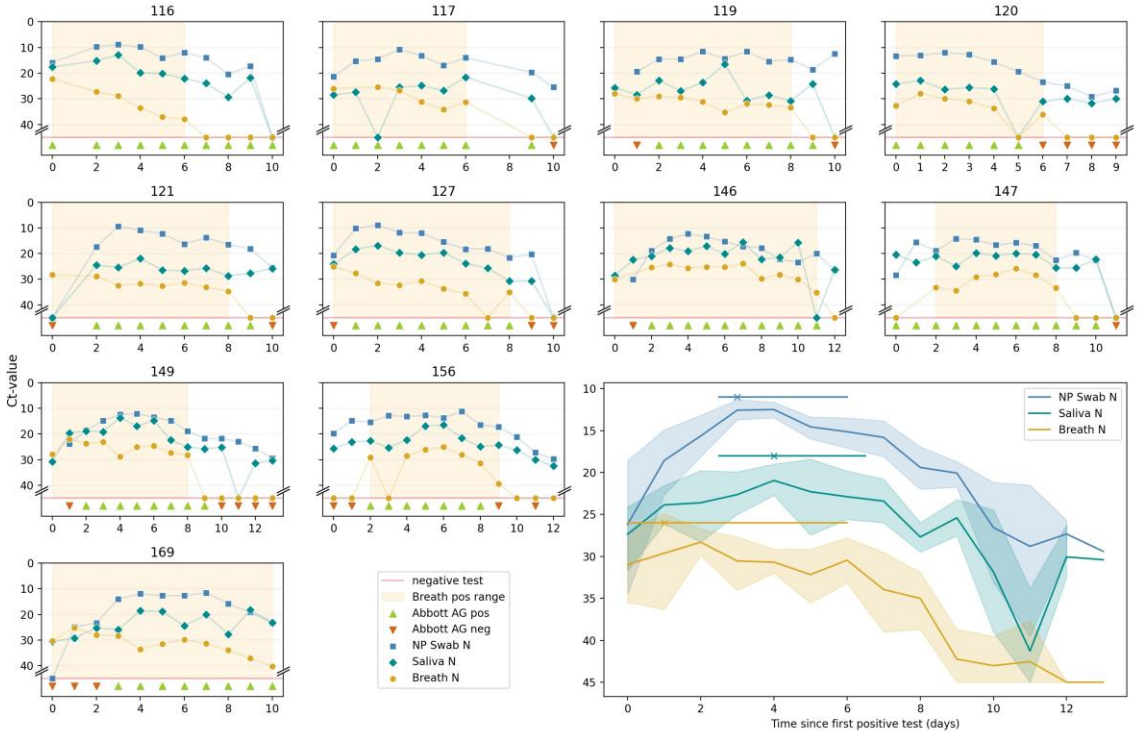

(a) Time since first positive test (days)

(b) Profile of Ct-values per test method

Fig. 3 summarizes the findings in the longitudinal study comparing Ct values of the N gene in breath (*breath test N*), nasopharyngeal swab (*NP Swab N*) and saliva (*saliva N*) to a rapid antigen test on nasopharyngeal swab (*Abbott AG*). **a**, Individual graphs of the 11 participants followed up over the course of their infection, day 0 being the first day any diagnostic test turned positive. The period in which the breath test is positive is shaded. As shown, 3/11 participants were positive on all tests concurrently, while 8/11 had discrepant results on the first day of testing positive. In the latter cases, the breath test turned positive before NP swab on two occasions (subject 121 and 169) and after on two others (subject 147 and 156). The Abbott AG test turned positive 0 to 3 days after a PCR test (mean 1.4 days). **b,** A summed graph in which the Ct values of all tests performed in the 11 participants on a particular day are averaged for one particular sample type. A trend towards an earlier peak in the breath test N in comparison to NP Swab N and saliva N is shown on top. Median and 95%CI were calculated using the bootstrap method. Lastly, as shown and more clearly visible from Extended Data Fig. 6, the breath test turns negative before RT-qPCR on other respiratory samples.

IN-SITU RAPID ON-CHIP RT-QPCR

The minute volume of the exhaled particle samples, in combination with the thermal properties of the silicon impactor chips, is ideally suited for conducting rapid and direct molecular tests at the point-of-need. To demonstrate this, an integrated workflow was designed, eliminating the need for a rinsing step after sampling (see Fig. 4). After sample collection, reagents were pipetted directly into the silicon impactor that filled by capillary actuation. The impactor was then sealed using a custom clamp (Fig. 4a), followed by a direct, in situ- RT-qPCR using a dedicated thermal cycler (see Fig. 4f). Results of the monolithic sieve were very similar to the non-monolithic approach using rinsing and off-sieve amplification (see Fig. 4d-e). Of the 40 clinical samples tested, 28 were positive and 5 were negative for both methods performed in duplicate. Of the remaining 7 samples, 1 sample was only positive on the non-monolithic sieve for currently unknown reasons. The other 6 samples showed non-identical duplicates, high Ct values, or a non-uniform amplification (i.e. discrete positive regions) on the monolithic sieve, all indications of the presence of very few viral copies and results being Poisson limited (see Supplementary Table **4**). Albeit currently still a close to 1 hour test, we already have used faster hardware to show that an ultrafast PCR can be performed on clinical samples on silicon with equal sensitivity[30]. Similarly, a sub-5 minutes RT-qPCR test was realized on a silicon chip for the detection of SARS-CoV-2 (Extended Data Fig. 3c-d) indicating the possibility of a rapid screening test for exhaled particles. Further development of the proposed platform for rapid testing will facilitate on-site testing and help to contain outbreaks as exemplified by the success of rapid antigen tests, with the added benefit of improved sensitivity and specificity of molecular testing[31]. Already in its current format, the platform could help to better understand the dynamics of

transmission by exhaled particles, not only for coronaviruses, but potentially for other airborne infectious diseases as well.

Fig. 4: In-situ RT-qPCR using an integrated, monolithic silicon chip.

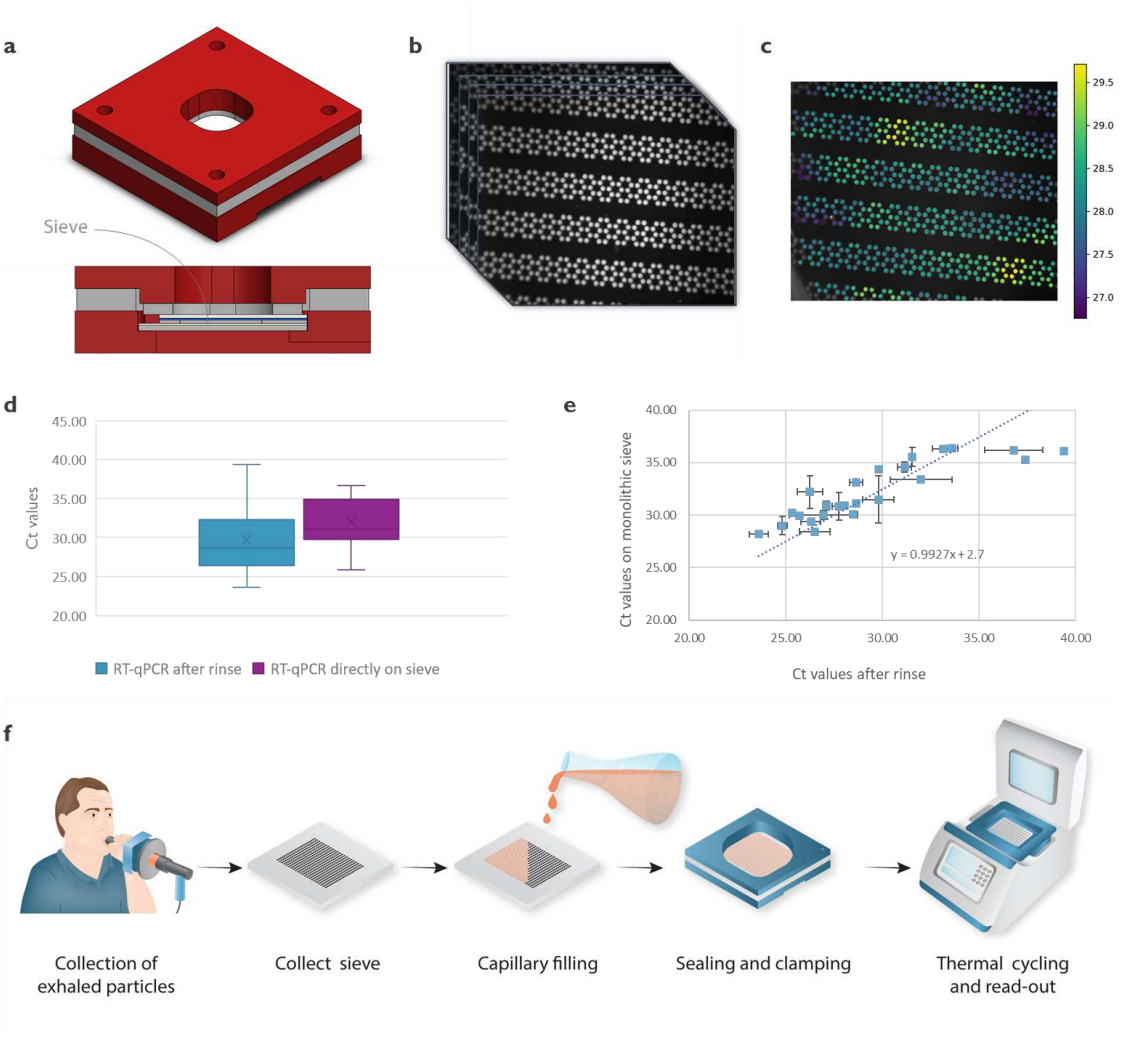

a, A 3D CAD image and cross-section of the clamped sieve. The poly-methyl-methacrylate (PMMA) housing has an opening on top for optical access and at the bottom for thermal access. The monolithic sieve itself is clamped in between a top glass substrate with a clear silicone sheet and a bottom silicon substrate with a Li2000 thermal tape for good thermal contact. More details of the housing and clamp are shown in Extended Data Fig. 4. **b**, The optical signal of the sieve is captured for each cycle during thermal cycling using an in-house developed RT-qPCR set-up resulting in series of images. **c**, Resulting heat-map of the fluorescent signals. An R-script is used to generate a Ct value for every nozzle/well. In the example shown, the median Ct value is 28.2 and the mean Ct value is 29.3, calculated over a total of 701 nozzles. **d**, Ct values obtained from the positive clinical samples comparing the rinsing method (mean 28.6) with the in-situ RT-qPCR method (mean 31.1). Note that the shift in Ct value was also apparent in the reference curves (see Extended Data Fig. 3b). **e**,

Scatterplot of the individual clinical samples that were positive for both RT-qPCR performed on the non-monolithic sieve with rinsing (x-axis) and monolithic sieve (y-axis) showing a linear relationship. The error bars represent the standard deviation from 2 samples gathered from the same subject at the same time point. **f**, Schematic overview of the used protocol for the monolithic version of the impactor. The monolithic sieve is removed from the sample device, followed by adding the master mix. The impactor fills by capillary fluidic movement after which both sides of the sieve are sealed using a PMMA clamp. The sieve with clamp is positioned in the custom thermal cycler for direct, in-situ RT-qPCR. More details of the set-up are shown in Extended Data Fig. 5.

CONCLUSION

Molecular tests on nasopharyngeal swabs have been the reference method for SARS-CoV-2 testing because of their purported sensitivity and specificity. Key disadvantages of this testing approach are that nasopharyngeal swab sampling is usually experienced as uncomfortable and requires a healthcare worker. Furthermore, it is prone to detecting viral particles that are no longer acutely infective. The difficulties to standardize sampling impact the reliability of measured viral concentrations[32]. Rapid antigen tests are preferred for their ease-of-use, but do not have the performance benefits of a molecular test. Most importantly, no existing test approach targets the actual mode of transmission, i.e. virus-laden exhaled particles. Some efforts have focused on analysing exhaled volatile organic compounds borne from the host response[33,34], providing indirect evidence of an infection. Using a novel sampling device, we have demonstrated a rapid, integrated workflow for the sensitive capture and molecular detection of virus particles in breath. While the detected viral concentrations show significant subject-to-subject variability, good reproducibility is obtained for a given subject over multiple days or when tested in duplicates. Vocalizing while exhaling appeared most sensitive amongst different breathing protocols tested, consistent with reports on the effect of vocalization on exhaled aerosol production[17,35] and anecdotal evidence of the importance of vocalization in superspreading events[36]. We demonstrated in a longitudinal study nearly on-par accuracy and sensitivity compared to the nasopharyngeal swab during the first week of an infection. Viral load assessed using the breath sample tends to peak earlier compared to and becomes undetectable before other sample types. These results suggest that the exhaled viral load decreases gradually over time after a peak early in the course of an infection. Since SARS-CoV-2 is believed to spread mostly by means of exhaled particles, the exhaled viral load may allow for a more accurate measurement of the actual transmission

window. We further show that both exhaled breath sampling and a fast RT-qPCR-based detection can be performed with a single silicon device. These results offer a path to the development of a non-invasive point-of-care molecular test for SARS-CoV-2 compatible with self-sampling. Our approach can readily be modified to detect other types of respiratory infectious agents and could be an effective means to control airborne infectious diseases.

METHODS

IMPACTOR DESIGN AND SIMULATIONS

The finite volume method and 3-D simulations of the impactor chip were performed using ANSYS Fluent commercial software. The discrete phase model (DPM) was used to track the particles' motion in the Lagrangian domain while the Eulerian formulation is simultaneously used for the continuous phase.[37] The pressure and velocity fields were calculated by solving the steady state laminar Navier-Stokes equation. The collection efficiency for a specific particle diameter was estimated by tracking the particles injected at the inlet of the nozzle using the DPM. The collection efficiency is the fraction of particles that are trapped on the impaction surface over the total number of particles injected. Because of the small size of tracked particles (<1um), the Cunningham correction factor had to be applied to the solution using a user defined function (UDF).[38]

FABRICATION OF THE SILICON IMPACTOR

To produce non-monolithic impactors, sieves were fabricated from 200 mm Si wafers using standard lithographic techniques. In short, after a standard clean to remove any particles, the Si wafers were patterned followed by a Bosch dry etch step using an SPTS tool, resulting in front side 30 µm deep shallow cavity. The cavity surface was then protected by a 200 nm thin thermal oxide layer. A temporary carrier was used to shield the front side cavity prior to grinding the wafers to 450 µm. The nozzles were then processed using back-side litho and etch landing on the shallow cavity. Afterward, the temporary carrier was removed using laser debonding. Extensive wet cleans followed by an ozone clean were applied to remove all the residues. The oxide to protect the Si surface was then removed by dipping the wafers

in a diluted (10% v/v) HF solution. A new 150 nm thin high quality oxide layer was formed by thermal oxidation at 1050 °C prior to standard dicing. It is expected that exhaled particles attach to any surface with which they come into contact, hence, no coating other than the silicon oxide finishing during processing was applied. A shown in Fig. 1, two sieve samples were mounted on top to create a fully functional impactor with a 30 µm gap. Monolithic impactors were fabricated on Si-Si fusion bonded 200mm wafers. The bottom wafers were first processed using deep reactive ion etching (DRIE) to form the 30 µm shallow cavity. After a thermal oxidation step to have a 200 nm thin oxide at the surface, these wafers were oxide-oxide fusion bonded with another blank Si wafer called top wafer. The top Si wafer was then grinded, resulting in a 100 µm thick membrane on top of the shallow cavity. Next, the top nozzles as well as the fluidic inlet/outlet were formed by a standard sequence of lithographic patterning followed by a dry etch step as described for the non-monolithic sieves. Next, a temporary carrier was used again to protect the holes at the top wafers, enabling backside grinding to 450 µm total Si-Si thickness and etching to form the backside nozzles. Special consideration was given to the timing of the backside etch to limit any over-etching. After removal of the temporary carriers, a sequence of wet clean steps followed, including a mesitylene and sulphuric acid-ozon clean, to remove all residues from temporary bonding process as well as passivation polymers from the bosh dry etch step. Finally, a new 150 nm thin high-quality oxide was formed by thermal oxidation and the wafers were diced to the final impactors (2x1.8 cm) used for testing (more info on the design and performance attributes of the monolithic impactors are shown in Extended Data Fig. 1).

IMPACTOR CAPTURE EFFICIENCY TESTS

To determine the capture efficiency of the breath sampler (see Fig. 2c and Extended Data Fig. 1), a nebulizer set-up was used to generate aerosols in a controlled manner. Aerosols were generated with an AGK2000 particle generator (Palas, Germany) from a 1.25 % KCl solution at 1 bar. The concentration of particles was adjusted by venting and diluting with air. Pneumatic switch valves enabled us to choose the flow path, and either went through an empty tube (control) or through our silicon chip. The aerosolized particle size distribution and concentration that left the control line or the chip was measured by a spectrometer Promo 2300 (Palas, Germany). The average concentration of particles arriving to the spectrometer during control $Cn_{aerosol}$ and during collection $Cn_{collection}$ was calculated. Collection efficiency was calculated as follows $(Cn_{aerosol-} Cn_{collection})/ Cn_{aerosol}$. The flow was regulated using an additional vacuum pump (RZ6 Vacuubrand), a flow meter and an adjustable flow restrictor allowing measurements from 5 L/min to 35 L/min.

IMPACTOR ACCEPTANCE MEASUREMENTS

A group of participants (N=32) was recruited to perform a series of breathing exercises in a lab setup created to determine the acceptable pressure drop for the sieve (see Fig. 2b). Participants were selected based on a short survey, taking into account differences in age, fitness and health conditions. Next to a group of healthy controls (N=12), the recruitment focused on profiles expected to have difficulties with performing the resistance tests, namely (1) elderly (N=8), (2) sedentary people (N=4) and (3) persons with respiratory difficulties (N=8). The lab setup (see Extended Data Fig. 2) included a spirometer and an adjustable valve to modify the pressure drop. Conditions with varying pressure drop were presented to participants in randomized order. Based on the spirometer data, a custom-built software

program provided feedback on their flow rate (target 0.6 L/s) and progress (target of 20 litres exhaled air). Following each exercise, participants rated subjective experience on a Likert scale ranging between 1 (very comfortable) to 7 (very uncomfortable), and perceived effort on a Borg scale ranging from 1 (very light activity) to 10 (max effort activity). To visualize the Likert data, a rating of 1-3 was recoded as comfortable, 4 as neutral, and 5-7 as uncomfortable. To adhere to hygienic and safety measures, a strict protocol was followed, including disinfection steps and disposable HEPA filters and mouthpieces. Participants received a small monetary reward in return.

RT-qPCR PROTOCOLS

For the nasopharyngeal and saliva samples, the standard validated protocol at University Hospitals Leuven was used. More specifically, the nasopharyngeal samples were collected in 1,5 mL zymo-medium (Zymo Research) and saliva samples (target 1.3mL) were collected in fertipro kits containing 2mL InactivBlue transport medium (InActiv Blue™). Sample transfer was performed using Tecan Evo200, Air liha. Extraction was performed using the KingFisher extraction robot. RT-qPCR was performed using the Taqpath 2019-ncov assay kit v2 (ThermoFisher) on 384-well plates using a Quantstudio 5 thermocycler. Analysis was performed using FastFinder analysis v4.x.

For the different generations of the impactor, slightly different direct (i.e. single step) RT-qPCR methods were used. The sequences of primers and probes are listed in Supplementary Table 1. For all protocols, a reference curve was obtained using synthetic RNA (Twist Biosciences) or genomic RNA (Vircell) (see Extended Data Fig. 3b). More specifically,

(1) for the non-monolithic impactor, a direct RT-qPCR was performed on the collected, exhaled particles. The RT-qPCR mix contained both primers (500nM 2019-nCoV_N2-F and 2019-nCoV_N2-R) and Taqman N2 probe (125nM) ordered from IDT (IDT, Belgium)

415 targeting the SARS-CoV-2 N2 gene, and feline infectious peritonitis virus (FIPV) primers
416 (FcoV1128f 400nM, FcoV1129r 900nM) and probes (250nM) and feline coronavirus
417 extracted RNA template (1e2 RNA copies per reaction) used as internal control.
418 The mix further contained ready to use RT-qPCR buffer (TaqPath™ 1-Step RT-qPCR
419 Master Mix, ThermoFisher) supplemented with 0.1% Triton X100 for virus lysis (see
420 Supplementary Info) and nuclease free water to a total volume of 50 µl. This mix was then
421 added to the surface of the bottom silicon sieve, on which the exhaled particles impacted.
422 After a short 2' incubation, the RT-qPCR mix was collected by briefly spinning the sieve
423 using a 50 mL plastic tube as a holder. The as such collected RT-qPCR mix was transferred
424 to PCR strips and loaded into a benchtop thermal cycler (LC96, Roche) for RT-qPCR (50°C
425 for 15' followed by 3' at 95°C and 50 cycles of 15" at 90°C and 60" at 60°C). The Cq values
426 were determined using the LightCycler application software.
427 (2) for the monolithic impactor and when using the custom instrument (see Extended Data
428 Fig. 5), a similar, somewhat faster protocol (30' qPCR) with minor modifications was used.
429 More specifically, the RT-qPCR protocol used similar N2 primers and probes, but at an
430 elevated concentration compared to the off-sieve PCR. The master mix contained 5 µM of
431 both 2019-nCoV_N2-F and 2019-nCoV_N2-R, 400nM N2 probe, 0.1U/µl KAPA2G HS fast
432 polymerase and TaqPath™ 1-Step RT-qPCR Master Mix supplemented with 1% Tergitol
433 15-S-9 for virus lysis. After an RT step of 15' at 50C, the mix was held at 95°C for 3',
434 followed by 45 PCR cycles (10" 60°C, 1" 95°C with a ramp rate of 10°C/s). The data
435 analysis is detailed in the Supplementary Info.
436 (3) for demonstrating an ultra-fast, below 5' RT-qPCR on chip, a further modified protocol
437 was developed as detailed in the Supplementary Info and results shown in Extended Data
438 Fig. 3c-d.

TRIAL DESIGN AND PARTICIPANTS: EXHALED PARTICLES SAMPLING IN HOSPITALIZED PATIENTS

The trial complied with the Declaration of Helsinki, the International Conference on Harmonization Guidelines for Good Clinical Practice, and applicable local regulations. The protocol was reviewed and approved by the ethics committee, and all subjects provided written informed consent before study entry. Subjects were recruited at the low-care covid ward at University Hospital Leuven (Belgium). For inclusion of SARS-CoV-2 positive subjects, patients hospitalized at the ward, either for COVID-19-related symptoms or for other health issues, were approached to participate in the study. All patients were aged 42 years or older, and tested positive for SARS-CoV-2 infection within 3 days of study inclusion. Both symptomatic and asymptomatic subjects were included. Specific symptoms were not systematically recorded. Patients with significant breathing problems were excluded from the study. A nasopharyngeal swab test was taken on the first day of inclusion in the study, and analysed with the reference RT-PCR test at the University Hospital to confirm the SARS-CoV-2 infection status. Healthy volunteers were recruited amongst the hospital staff at the low-care covid ward. At the time of this study, no subjects had received a vaccine or had confirmed previous SARS-CoV-2 infection.

After enrolment, study participants were asked to breathe into the breath sampler. A breathing test was defined as 20 tidal exhalations through the breath sampler, while the air flow was measured with a spirometer. During the breathing test, all subjects were instructed to stay within their comfort levels, and thus the air flow was variable in this study. In all cases, the subjects were instructed to exhale into the mouthpiece of the breath sampler and inhale away from the device or through the nose. Subjects were asked to repeat the breathing test typically 2 times. A number of patients were tested again up to 4 days later.

TRIAL DESIGN AND PARTICIPANTS: EXHALED PARTICLES SAMPLING IN STUDENT TESTING CENTRE

The trial complied with the Declaration of Helsinki, the International Conference on Harmonization Guidelines for Good Clinical Practice, and applicable local regulations. The protocol was reviewed and approved by the ethics committee, and participants provided written informed consent before study entry.

In order to be included in the study, the subjects had to be tertiary education students residing in Leuven, Belgium, who wanted to be tested following a high-risk contact, symptoms typical of a SARS-CoV-2 infection, or after returning from a high-risk country. For the selection of subjects, a combination of risk assessment (questionnaire) and pre-selection through rapid tests (Abbott Panbio Covid 19 Ag testkit) was used. As the students were sampled using a nasopharyngeal swab test, the result of this test was used as reference. It should be noted that even subjects selected as a "negative subject" were still at risk of being positive. The clinical study contained 3 parts: (1) a comparison of different breathing techniques, (2) a longitudinal study, following subjects over multiple days with multiple tests daily and (3) a comparison between on-sieve and off-sieve RT-qPCR methods.

(1) For comparison of breathing techniques, volunteering students were asked to breathe through the sieve using different breathing methods (4 min tidal breathing; 2 min tidal breathing; 1 min exhaling accompanied by the sound "e"; 10 deep exhalations into the device). In all cases, the subjects were instructed to alternatingly exhale into the mouthpiece and inhale away from the device or via the nose. Subjects were asked never to go beyond their comfort zone and could stop at any moment.

(2) For the longitudinal study, subjects were screened for recruitment by the KU Leuven contact tracing team focusing on contact tracing of the Leuven tertiary education student population[16]. Subjects needed to be recently exposed to a confirmed COVID-19 case.

Preferentially, this source case had a high viral load and had likely caused a secondary infection already. Exclusion criteria were: previous vaccination or COVID-19 infection (based on previous positive RT-qPCR test or antibody test at inclusion), exposure more than 7 days prior to assessment for inclusion, physical inability to attend the testing centre or inability to provide informed consent. Participants were preferentially recruited if they were thought to be in an early phase of infection based on initial diagnostic tests, symptom onset and exposure history. Saliva (saliva N) and breath RT-qPCR (breath test N) were performed once to twice daily while a nasopharyngeal RT-qPCR (NP Swab N) and antigen (Abbott AG) test were performed once daily. Participants remaining negative were excluded 5 to 7 days after exposure. Participants who tested positive during follow-up were initially asked to provide breath and saliva samples twice daily. However, intermediate data analysis revealed limited variation in same day Ct values, prompting a switch to once daily sampling of subjects for all diagnostic tests. Symptoms were not systematically recorded. When participants remained positive on at least one of the performed tests until day 10, follow up was prolonged until subjects were deemed unlikely to still be infectious by a medical doctor based on Ct values and symptom resolution. Due to the availability of the subject or test taker, no sample was taken on a limited number of days. The selection procedure and inclusion flowchart are visualised in Extended Data Fig. 7.

(3) For the comparison between on-sieve and off-sieve RT-qPCR, SARS-CoV-2 positive subjects were asked to breathe through the 2 different systems, using the vocalization protocol. Each method was repeated twice, resulting in a total of 4 datapoints per subject.

511

512 ## REFERENCES

513 1. Greenhalgh, T. *et al.* Ten scientific reasons in support of airborne transmission of
514 SARS-CoV-2. *Lancet* **397**, 1603–1605 (2021).

515 2. Vuorinen, V. *et al.* Modelling aerosol transport and virus exposure with numerical
516 simulations in relation to SARS-CoV-2 transmission by inhalation indoors. *Saf. Sci.*
517 **130**, 104866 (2020).

518 3. Taylor, D., Lindsay, A. C. & Halcox, J. P. Aerosol and Surface Stability of SARS-CoV-2
519 as Compared with SARS-CoV-1. *NEJM* 0–2 (2020).

520 4. Lednicky, J. A. *et al.* Viable SARS-CoV-2 in the air of a hospital room with COVID-19
521 patients. *Int. J. Infect. Dis.* **100**, 476–482 (2020).

522 5. Tang, J. W., Marr, L. C., Li, Y. & Dancer, S. J. Covid-19 has redefined airborne
523 transmission. *BMJ* **373**, 1–2 (2021).

524 6. Lemieux, J. E. *et al.* Phylogenetic analysis of SARS-CoV-2 in Boston highlights the
525 impact of superspreading events. *Science (80-.).* **371**, (2021).

526 7. Raymenants, J., Geenen, C., Gorissen, S. & André, E. Empirical evidence on the
527 efficiency of bidirectional contact tracing in COVID-19. 1–16 (2021).

528 8. Kevadiya, B. D. *et al.* Diagnostics for SARS-CoV-2 infections. *Nat. Mater.* **20**, 593–605
529 (2021).

530 9. Takeuchi, Y. *et al.* Diagnostic performance and characteristics of anterior nasal
531 collection for the SARS-CoV-2 antigen test: a prospective study. *Sci. Rep.* **11**, 1–8
532 (2021).

533 10. Giovannini, G., Haick, H. & Garoli, D. Detecting COVID-19 from Breath: A Game
534 Changer for a Big Challenge. *ACS Sensors* **6**, 1408–1417 (2021).

535 11. Verreault, D., Moineau, S. & Duchaine, C. Methods for Sampling of Airborne Viruses.

536 *Microbiol. Mol. Biol. Rev.* **72**, 413–444 (2008).
537 12. Ryan, D. J. *et al.* Use of exhaled breath condensate (EBC) in the diagnosis of SARS-
538 COV-2 (COVID-19). *Thorax* **76**, 86–88 (2021).
539 13. Malik, M., Kunze, A. C., Bahmer, T., Herget-Rosenthal, S. & Kunze, T. SARS-CoV-2:
540 Viral Loads of Exhaled Breath and Oronasopharyngeal Specimens in Hospitalized
541 Patients with COVID-19. *Int. J. Infect. Dis.* **110**, 105–110 (2021).
542 14. Smolinska, A. *et al.* The SARS-CoV-2 viral load in COVID-19 patients is lower on face
543 mask filters than on nasopharyngeal swabs. *Sci. Rep.* **11**, 13476 (2021).
544 15. Kenyon, C. The prominence of asymptomatic superspreaders in transmission mean
545 universal face masking should be part of COVID-19 de-escalation strategies. *Int. J.*
546 *Infect. Dis.* **97**, 21–22 (2020).
547 16. Raymenants, J., Geenen, C., Thibaut, J., Gorissen, S. & Nelissen, K. Integrated PCR
548 testing and extended window contact tracing system for COVID-19 to improve
549 comprehensiveness and speed. *Protoc. Exch.* (2021) doi:10.21203/rs.3.pex-1666/v1.
550 17. Asadi, S. *et al.* Aerosol emission and superemission during human speech increase
551 with voice loudness. *Sci. Rep.* **9**, 1–10 (2019).
552 18. Chen, P. Z. *et al.* Heterogeneity in transmissibility and shedding SARS-CoV-2 via
553 droplets and aerosols. *Elife* **10**, 1–32 (2021).
554 19. Chen, P. Z. *et al.* SARS-CoV-2 shedding dynamics across the respiratory tract, sex,
555 and disease severity for adult and pediatric COVID-19. *Elife* **10**, (2021).
556 20. Edwards, D. A., Ausiello, D., Salzman, J., Devlin, T. & Langer, R. Exhaled aerosol
557 increases with COVID-19 infection , age , and obesity. **118**, 1–7 (2021).
558 21. Yan, J. *et al.* Infectious virus in exhaled breath of symptomatic seasonal influenza cases
559 from a college community. *Proc. Natl. Acad. Sci. U. S. A.* **115**, 1081–1086 (2018).
560 22. Leung, N. H. L. *et al.* Respiratory virus shedding in exhaled breath and efficacy of face

masks. *Nat. Med.* **26**, 676–680 (2020).

23. Dinnes, J. *et al.* Rapid, point-of-care antigen and molecular-based tests for diagnosis of SARS-CoV-2 infection. *Cochrane Database Syst. Rev.* **2020**, (2020).

24. Mancuso, P. *et al.* Temporal profile and determinants of viral shedding and of viral clearance confirmation on nasopharyngeal swabs from SARS-CoV-2-positive subjects: A population-based prospective cohort study in Reggio Emilia, Italy. *BMJ Open* **10**, (2020).

25. Hu, S. *et al.* Infectivity, susceptibility, and risk factors associated with SARS-CoV-2 transmission under intensive contact tracing in Hunan, China. *Nat. Commun.* **12**, 1–11 (2021).

26. Cheng, H. Y. *et al.* Contact Tracing Assessment of COVID-19 Transmission Dynamics in Taiwan and Risk at Different Exposure Periods before and after Symptom Onset. *JAMA Intern. Med.* **180**, 1156–1163 (2020).

27. Perera, R. A. P. M. *et al.* SARS-CoV-2 Virus Culture and Subgenomic RNA for Respiratory Specimens from Patients with Mild Coronavirus Disease. *Emerg. Infect. Dis.* **26**, 2701–2704 (2020).

28. Wölfel, R. *et al.* Virological assessment of hospitalized patients with COVID-2019. *Nature* **581**, 465–469 (2020).

29. Bullard, J. *et al.* Predicting infectious severe acute respiratory syndrome coronavirus 2 from diagnostic samples. *Clin. Infect. Dis.* **71**, 2663–2666 (2020).

30. Cai, Q. *et al.* Ultra-fast, sensitive and quantitative on-chip detection of group B streptococci in clinical samples. *Talanta* **192**, (2019).

31. Hu, Y. *et al.* Role of efficient testing and contact tracing in mitigating the COVID-19 pandemic : a network modelling study. 1–13 (2021) doi:10.1136/bmjopen-2020-045886.

586 32. Higgens, T. S., Wu, A. W. & Ting, J. Y. Comparison of nasopharyngeal aspirate with
587 flocked swab for PCR-detection of respiratory viruses in children. *Apmis* **123**, 473–
588 477 (2015).
589 33. Ibrahim, W. *et al.* Diagnosis of covid-19 by exhaled breath analysis using gas
590 chromatography–mass spectrometry. *ERJ Open Res.* **7**, (2021).
591 34. Chen, H. *et al.* COVID-19 screening using breath-borne volatile organic compounds. *J.*
592 *Breath Res.* (2021) doi:10.1088/1752-7163/ac2e57.
593 35. Gregson, F. K. A. *et al.* Comparing aerosol concentrations and particle size
594 distributions generated by singing, speaking and breathing. *Aerosol Sci. Technol.* **55**,
595 681–691 (2021).
596 36. Hamner, L. *et al.* High SARS-CoV-2 Attack Rate Following Exposure at a Choir
597 Practice - Skagit County, Washington, March 2020. *MMWR. Morb. Mortal. Wkly. Rep.*
598 **69**, 606–610 (2020).
599 37. Zahari, N. M. *et al.* Introduction of discrete phase model (DPM) in fluid flow: A
600 review. *AIP Conf. Proc.* **2030**, (2018).
601 38. Gussman, R. A. On the Aerosol Particle Slip Correction Factor. *J. Appl. Meteorol.*
602 *Climatol.* **8**, 999–1001 (1969).
603 39. Ritz, C. & Spiess, A. N. qpcR: An R package for sigmoidal model selection in
604 quantitative real-time polymerase chain reaction analysis. *Bioinformatics* **24**, 1549–
605 1551 (2008).
606
607

ACKNOWLEDGEMENTS

We want to thank Hanne Lenaerts, Chris D'haemer, Sabine Clabots, Hannelore De Mulder, Zakia Madour, Soumia El Mahmoudi, Mehdi Humbert, and Pieter-Jan Eelen for help during the clinical tests and breath sampler assembly; Karen Van Keer for facilitating lab tests; Younjae Choe, Antonio Pappaterra, Comate Engineering & Design and EXD Excogitate design for help in designing the breath sampler housing and clamp; Somersault1824 for help in art work; and Virovet Livestock Solutions for help with feline virus tests. The work was partially funded by a project grant of the Flemish Government. PB acknowledges support of the Research Foundation Flanders (FWO, grant number: 1S89519).

ETHICS

The clinical studies were set up via the Ethical Commission of UZ Leuven: OMAKA pilot study: In-vitro Validation of imec Aerosol Sieve for Capturing SARS-CoV-2 Virus (study reference S64765); YAS Open-label PoC study: IMEC Breath Sampler for Capturing and Detecting SARS-CoV-2 Virus in Aerosols and Droplets of Exhaled Breath" (study reference S65005).

SUPPLEMENTARY DATA

Virus lysis results

To enable direct RT-qPCR on sieve, different methods to directly lyse the virus prior to and during the RT step were tested. A feline coronavirus (FIPV) viral culture -kindly provided by Virovet Livestock Solutions- was initially used as a SARS-CoV-2 mimic and observed results were later confirmed using a SARS-CoV-2 viral culture for the final concentrations used during the tests. From all detergents tested, Triton-X100 (and later Tergitol 15-S-9 as a replacement) gave the best results, not inhibiting PCR until at least a concentration of 1%, and showed complete lysis from concentrations as low as 0.05% upwards (see Extended Data Fig. 3a). The addition of these detergents to the master mix enabled the direct single-step RT-qPCR on the collected samples without the need for RNA extraction.

Primer sequences

Supplementary Table 1: Sequences of the used primers and probes listed along with their references.

Name of target (reference)	Sequence (5' → 3')
FIPV (doi: 10.1016/S0166-0934(98)00129-3)	
FcoV1128f	5' GATTTGATTTGGCAATGCTAGATTT
FcoV1229r	5' AACAATCACTAGATCCAGACGTTAGCT
FIPV probe	5' HEX- TCCATTGTT/ZEN/GGCTCGTCATAGCGGA-ZEN/IBFQ
SARS-CoV-2 N1 (https://www.cdc.gov/coronavirus/2019-ncov/lab/rt-pcr-panel-primer-probes.html)	
2019-nCoV_N1-F	5' GAC CCC AAA ATC AGC GAA AT
2019-nCoV_N1-R	5' TCT GGT TAC TGC CAG TTG AAT CTG
N1 probe	5' FAM-ACC CCG CAT TAC GTT TGG TGG ACC-BHQ1
SARS-CoV-2 N2 (https://www.cdc.gov/coronavirus/2019-ncov/lab/rt-pcr-panel-primer-probes.html)	
2019-nCoV_N2-F	5' TTA CAA ACA TTG GCC GCA AA
2019-nCoV_N2-R	5' GCG CGA CAT TCC GAA GAA

	N2 probe	5' FAM-ACA ATT TGC CCC CAG CGC TTC AG-BHQ1

Fast RT-qPCR on chip

In order to demonstrate the potential for a reduced overall turn-around-time from sample collection to the availability of a result, a rapid RT-qPCR was developed in parallel. Fast thermal cycling was performed by mounting a silicon chip with a PCR cavity on top of a thermo-electric cooler (MPC701, Micropelt), as shown in Extended Data Fig. 3c-d, in agreement with our earlier reported data[19]. A similar RT-qPCR master mix was used as in the off-sieve analysis method, but with an increased concentration of primers (20 µM of both 2019-nCoV_N1-F and 2019-nCoV_N1-R) and probe (500nM of N1 probe) as well as the addition of extra polymerase (1.68 units/µL of KAPA2G HS fast polymerase, Kapa Biosystems, USA). The RT-qPCR mixtures were pipetted into the reaction chamber of the chip and different concentrations of purified genomic SARS-CoV-2 RNA (Vircell) were used. The RT-qPCR consisted of a 1-minute RT-step at 50°C, followed by a 20" denaturation step and 46 cycles of 5 sec (1" heating, 2" cooling, 2" hold at 60°C) resulting in a ~5' total PCR time. Fluorescence measurements during every cycle were extracted by determining the mean grayscale value using ImageJ software. The raw data was used to determine the Ct value by the crossing point method I6 from the qpcR package in R[39].

Breath sampler detailed description and assembly

The disposable breath samplers used to capture exhaled particles during clinical testing are shown in Extended Data Fig. 4. The subjects were asked to breath or vocalize though a 1-way mouthpiece (Clement Clarke), connected to the custom housing and aluminium casing for the silicon impactor. Upon exiting the housing through the rear end, the exhaled breath passed through a filter (Piston Medical PBF-100-G-C) as an extra safety measure for

665 the test-taker. Finally, a connected spirometer (Pasco) was used to monitor the flow during
666 the breathing manoeuvre as a quality control. To avoid breath condensate blocking the
667 nozzles of the silicon sieves, the breath samplers were preheated at 70°C for at least 90'
668 and transported in a hotbox at the same temperature. After removal of the breath sampler
669 from the box, the aluminium casing ensured the sieve to remain above 37°C for another
670 40', sufficiently long for a test to be completed (see Extended Data Fig. 4c). A similar
671 procure was followed for the non-monolithic and the monolithic impactors.
672
673 ## Clamp for monolithic chip and mounting protocol
674 To hermetically seal and mount the monolithic chip in the thermal cycler, a plastic clamp
675 was designed (Extended Data Fig. 4g-h). The PMMA clamp was fabricated by CNC milling
676 (Protolabs). A silicon piece laminated with Li2000A thermal tape was glued to the bottom
677 part of the clamp. The silicon piece is in direct contact with the thermo-electric cooler of
678 the thermal cycler during RT-qPCR. On top of these layers the filled sieve was placed,
679 followed by a silicone sheet and a glass window for optical access. The steps used to mount
680 the sieve prior to thermal cycling are shown and explained in Extended Data Fig. 4g.
681
682 ## In-house developed thermal cycler for monolithic chip tests
683 A custom instrument Extended Data Fig. 5 was developed to execute RT-qPCR tests
684 directly on the silicon impactor chip according to the protocol optimized for the assay
685 requirements (see Extended Data Fig. 5). The instrument consists of two main subsystems: a
686 thermal module and an optical module. First, the thermal subsystem is composed of a
687 temperature controller (Accuthermo FTC200) and a Peripheral module that integrates a
688 Peltier element (Marlow Industries XLT3-4-01LS) as heating actuator, a liquid cooler unit
689 (Corsair H45) for rapid temperature cycling, and a thermocouple (Omega CHAL-003-BW)

for temperature feedback. This module also includes the necessary power and controller electronics to ensure a closed loop control over the temperature of the chip during a RT-qPCR run. Second, the optical subsystem comprises a custom-built inverted wide-field fluorescence microscope. It utilizes a 2X objective lens, a CMOS camera (Ximea MQ013MG-ON) and an LED illuminator (Thorlabs LED470L). The illumination and collection optics are designed to excite FAM fluorophore and collect fluorescence signals to observe DNA synthesis during RT-qPCR. Once the chip clamp assembly is mounted and set in position, the optical imaging system has the chip surface in focus such that approximately 7 x 7 mm^2 of the surface area of the chip is imaged in synchronization with thermal cycles with sufficient optical resolution and depth of focus to discern the signal of individual wells/nozzles.

The controller units of the subsystems are connected to a PC and a custom LabView software is built to realize a graphical-user-interface (GUI) and to control the hardware components. The GUI allows an operator to set a standard operating recipe such as thermal cycling parameters (e.g. duration and temperature set points during initialization, denaturation, annealing and extension phases of the RT-qPCR) and the optical parameters (e.g. camera exposure). Furthermore, the operator can also monitor the progress of the RT-qPCR run in the GUI and can intervene with the experiment if an unexpected event occurs during the operation.

Data analysis for the monolithic chip

After each RT-qPCR run, the raw data (e.g., optical images, data log files, etc.) were uploaded to a remote server on which a custom developed data processing software pipeline written in Python was executed to extract qPCR metrics such as Ct values from recorded images and meta data. This post-processing involves various image and signal

processing steps. A high-level overview of the pipeline is shown in Extended Data Fig. 5d. In a nutshell, the recorded images are first checked for irregularities such as trapped air bubbles in a well of the chip. Then, the fluorescence data series per qPCR cavity are generated. The wells with irregular signal behaviours such as flat signal curves are located and singled out. Once the signal data series are obtained per well, a six-parameter log logistic non-linear sigmoidal model was fitted per well through solving a non-linear least squares problem. The fit results are also evaluated in terms of errors and confidence ranges. The Ct values and efficiency values were calculated using the fitted models. The method is repeated for each well detected in the images (typically several hundreds) and averages and distributions are calculated per chip. The data analysis tool allows the expert user to interrogate the qPCR curves and allows for deriving global statistics from the entire chip. The whole analysis can be performed in less than half a minute and can be further optimized for speed.

Trial: exhaled particle sampling in hospitalized patients

As described in the methods and results sections, in this study a total of 55 subjects of which 23 were healthy volunteers were enrolled. For the positive subjects and as shown in the table below, an overall 75 % positive agreement was observed between the breath and nasopharyngeal RT-qPCR test.

Supplementary Table 2: Results for the first clinical study, where nasopharyngeal swab tests were compared to the breathing tests. Left: overview of the study set-up. 55 patients were sampled of which 32 were positive using the nasopharyngeal swab tests while the others were healthy volunteers. Right: The numbers resulting in the calculated percentage positive and negative agreement are listed. The corresponding, observed Ct values are available in the source data 1 file.

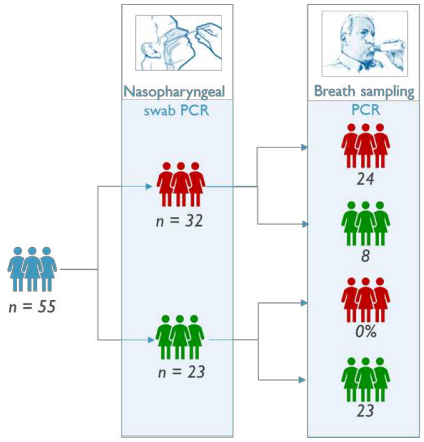

	Nasopharyngeal	Breath
POS, in agreement	32	24
POS, no agreement	0	8
NEG, in agreement	23	23
NEG, no agreement	0	0
TOTAL		
Positive agreement % (Sensitivity)	**100%**	**75%**
Negative agreement % (Specificity)	100%	100%

Trial: comparison of breathing protocols

To compare four different breathing methods, we enrolled a total of 56 subjects. As shown in the table below, when comparing the 4 breathing methods in the student population, vocalization was clearly the best method, with a percentage positive agreement of 74% and a percentage negative agreement of 100%. Nasopharyngeal swab was used as non-reference method and thus has 100% agreement. Note that the antigen test results also perform very well as they were used as the main selection criteria to enrich the subjects participating for this particular study.

Supplementary Table 3: Results for the clinical test where four different breathing methods were compared and a nasopharyngeal swab test was taken as control. Left: overview of the study set-up. 56 patients were sampled of which 23 were positive using the nasopharyngeal swab tests while the others were negative. Right: The numbers resulting in the calculated percentage positive and negative agreement are listed. As shown, vocalization clearly gives the best % positive agreement compared to the other breathing methods. The corresponding, observed Ct values are available in the source data 2 file.

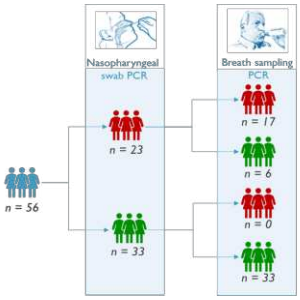

	NP swab PCR	Antigen	4 min	2 min	Vocalization	10x
POS, in agreement	23	22	9	6	17	5
POS, no agreement	0	1	1	1	0	0
NEG, in agreement	33	32	32	33	32	31
NEG, no agreement	0	1	14	16	6	18
TOTAL	56	56	56	56	55	54
Positive agreement % (Sensitivity)	**100%**	**96%**	**39%**	**26%**	**74%**	**22%**
Negative agreement % (Specificity)	100%	97%	97%	97%	100%	100%

Trial: Comparison non-monolithic vs. monolithic results

As shown in Fig. 4d-e, a nearly perfect linear correlation existed between the positive samples of the monolithic (i.e. encompassing a single Si chip) and non-monolithic (i.e. encompassing 2 silicon chips stacked on top of each other) sieves. Some samples, however, gave different results between the two impactors. As shown in the Supplementary Table 4 below, this was especially the case - except for sample 1- for samples yielding results with an estimated total of less than 10 viral copies collected on the impactor sieve.

Supplementary Table 4: Expected viral copies calculated based on reference curves for the observed Ct values. For the monolithic sieve, no copies were indicated as all positives samples in the table below showed a non-uniform amplification on chip with clear positive next to negative areas indicating a low, discrete number of copies.

Sample	Non-monolithic viral copies (Ct)		Monolithic sieve	
1	12 (34.4)	17 (33.8)	Neg	Neg
2	2 (37.0)	Neg	Neg	Neg
3	Neg	31 (33.5)	Pos	Pos
4	4 (37.4)	Neg	Pos	
5	1 (38.1)	Neg	Neg	Neg
6	Neg	1 (39.4)	Pos	
7	Neg	Neg	Pos	Neg

775 -

776 EXTENDED DATA FIGURES

777 **Extended Data Fig. 1: Monolithic impactor design and characteristics.**

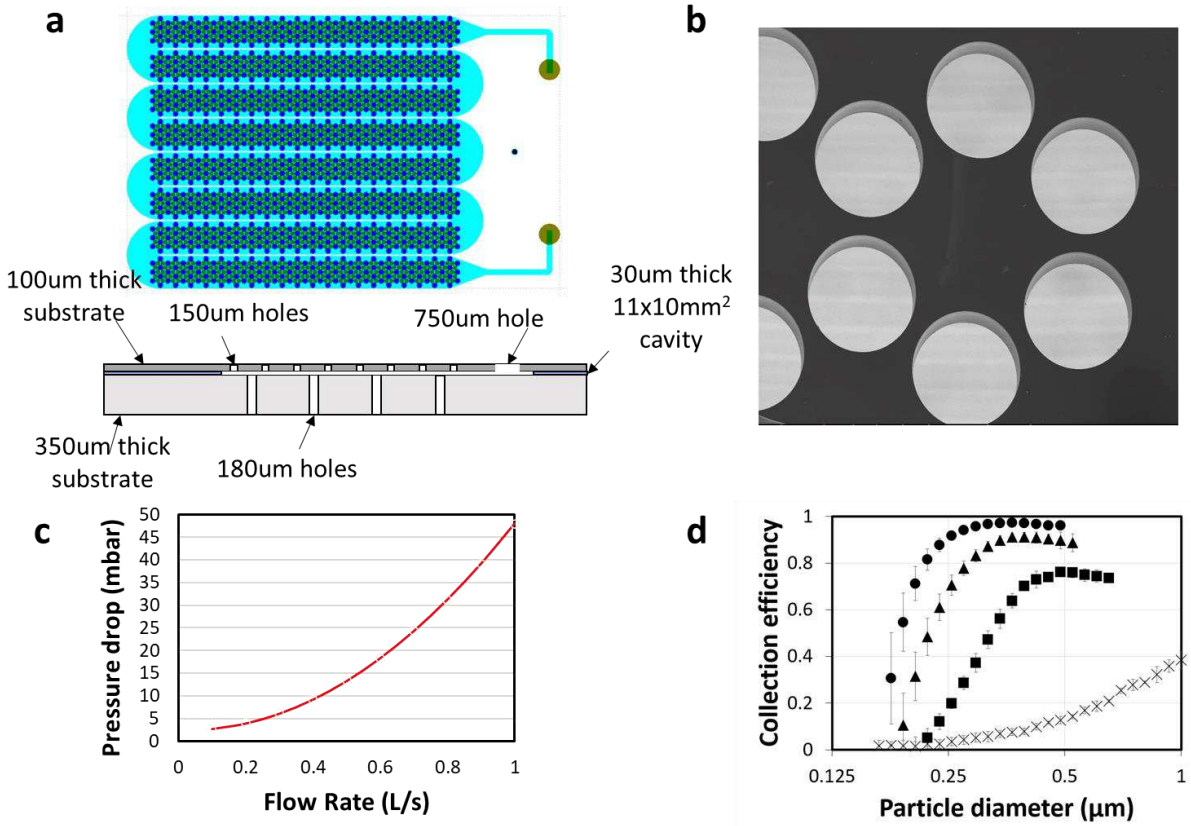

778

779 **a**, Design and cross-section with indicated dimensions of the monolithic impactor. As shown the 1600 inlet
780 nozzles have a diameter of 150 µm, while the 1144 outlet nozzles have a diameter of 180 µm. The inlet and
781 outlet nozzles are separated 20 µm apart. The impactor has a total volume of 15.8 µl of which 2.9 µl from the
782 inlet nozzles, 3.6 µl from the central cavity, and 9.3 µl from the outlet nozzles. **b**, SEM picture of the 150 µm
783 wide inlet nozzles of the fabricated monolithic impactor imaged from the top. **c**, Simulated pressure drop
784 versus flow rate for the monolithic chip, designed to match the non-monolithic chip. **d**, The measured
785 normalized capture efficiencies of the impactor in function of particle diameter for different flow rates (circles:
786 0.6 L/s, triangles : 0.42 L/s, squares : 0.25 L/s, crosses : 0.08 L/s).

787

788

Extended Data Fig. 2: Test set-up used for the impactor resistance and acceptance tests.

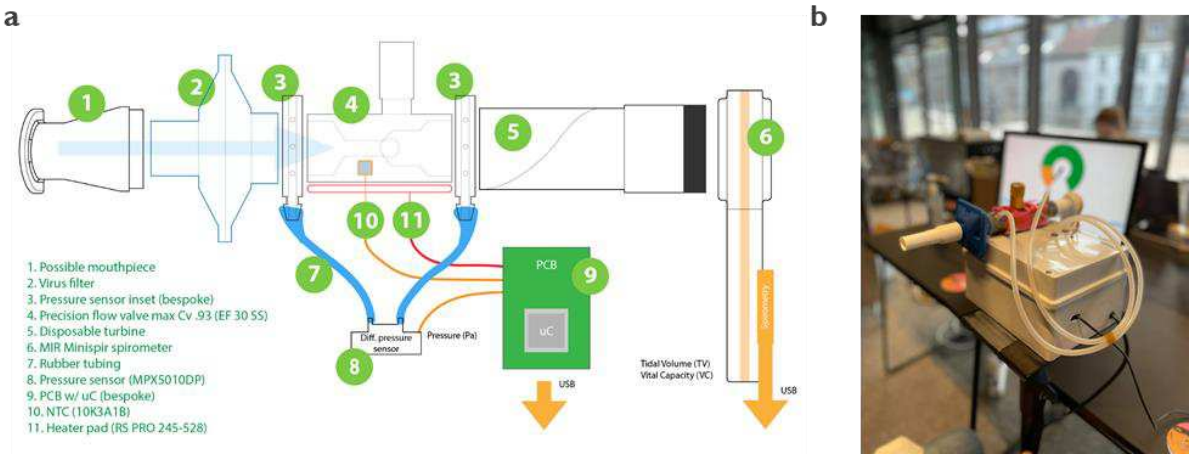

a, Schematic overview of the test set-up and its components. The components are listed in the legend. An adjustable valve (4) was used to change the resistance during exhalation. Subjective experience was rated on a Likert scale ranging between 1 (very comfortable) to 7 (very uncomfortable) and recoded into 3 comfort categories (comfortable, neutral and uncomfortable) as shown in Fig. 2b. Perceived effort was rated on a Borg scale ranging between 1 (very light activity) to 10 (maximal effort activity). Ratings varied between light activity (average rating of 2.2) for the lowest resistance setting (~20 mbar) to vigorous activity (average of 7.9) for the highest resistance setting (~60 mbar). **b**, Picture of the actual set-up, including the PC monitor showing the user interface with direct feedback to the volunteers on the achieved flow rate and progression.

Extended Data Fig. 3: Virus lysis data, RT-qPCR standard curves, and fast RT-qPCR on chip.

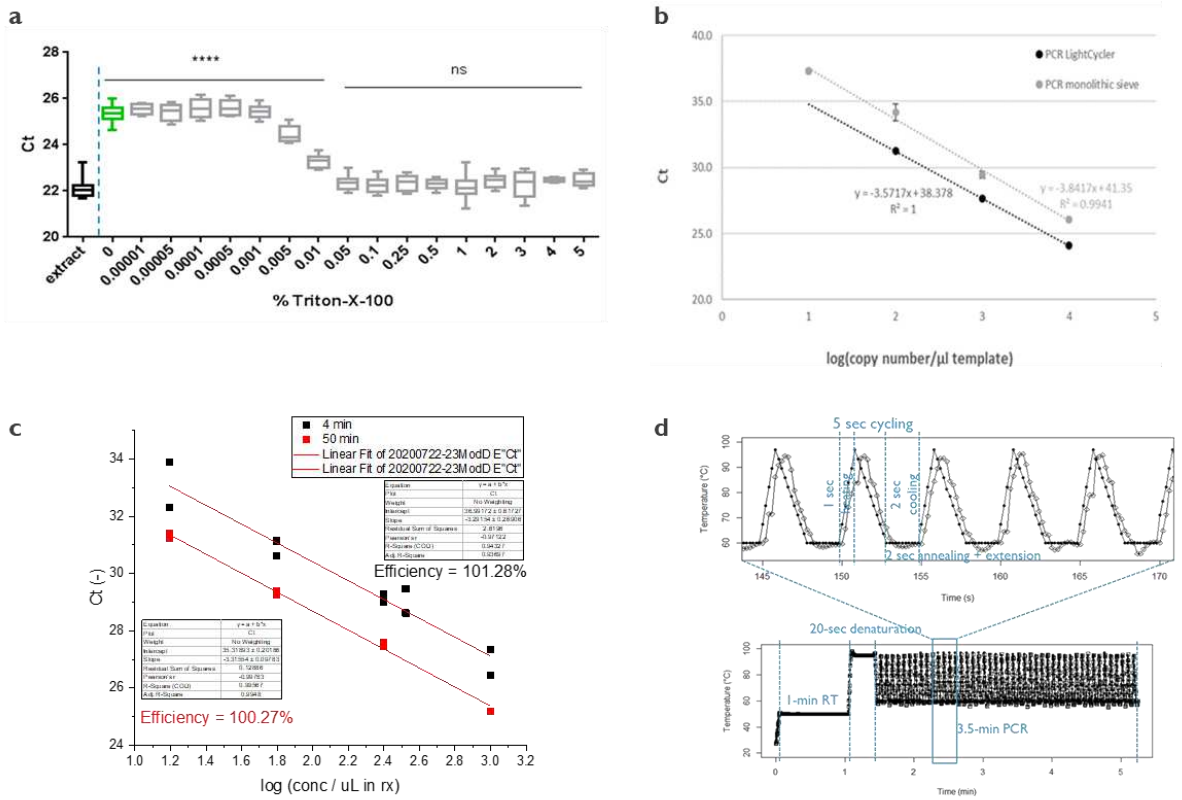

a, Virus lysis experiments using different concentrations of Triton-X100. The observed Ct values for RT-qPCR are shown after brief incubation with the Triton-X100detergent using FIPV virus as a SARS-CoV-2 mimic. Extracted RNA from the same virus stock and pure virus stock without Triton-X100 were included as positive and negative control, respectively. The **** indicate a significant difference ($p<0.05$), while ns indicates a non-significant difference compared to the positive control. A similar trend was observed for Tergitol 15-S-9 (not shown). **b**, RT-qPCR standard curves using different concentrations RNA genomic template (N > 2) for both LightCycler (black) and the monolithic sieve (grey) using the in-house developed PCR instrument. The concentration versus observed Ct values are calculated and plotted using the L6 R-script as described. The linear trendline for the 10-fold dilutions is plotted as well. As shown an upward shift in Ct values was observed, similar to the results observed during the clinical tests. **c**, RT-qPCR standard curves using different concentrations RNA genomic template using both a standard (in red, 50min) protocol and a fast (in black, 5min) protocol using silicon chips described previously[30]. **d**, Detailed overview of the programmed and

819 measured temperature profile for the fast RT-qPCR showing a 1 sec heating step, 2 sec cooling step, and 2 sec
820 elongation step per cycle (46 PCR cycles in total). The total reaction times for all steps are indicated.
821
822

Extended Data Fig. 4: Images of breath sampler and its components for the monolithic and non-monolithic impactor along with its assembly.

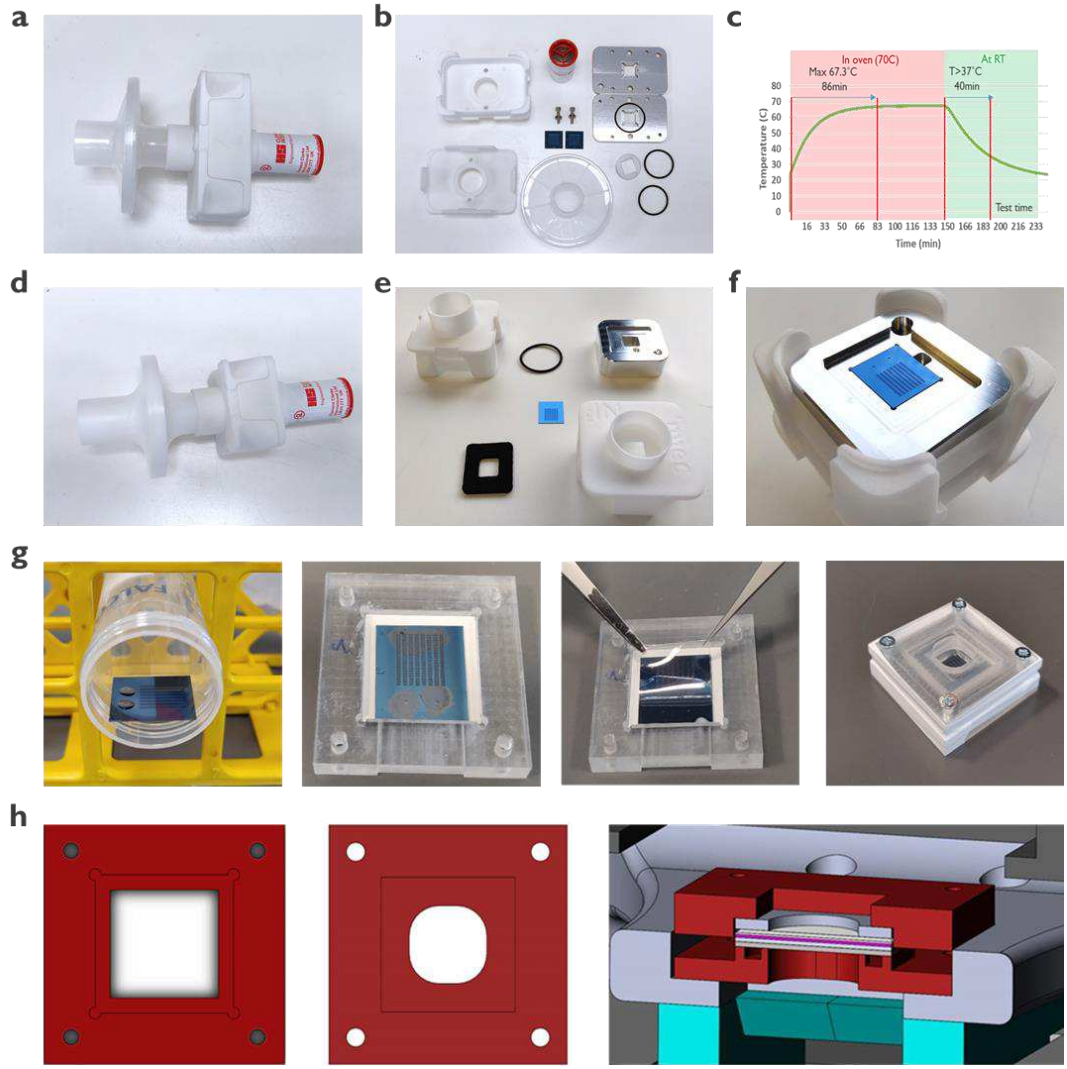

a, Picture of the breath sampler for the non-monolithic sieve, including single-use mouth piece (Clement Clarke), custom PMMA housing, and viral filter (Piston Medical PBF-100-G-C) which is mounted on a spirometer during clinical tests (Pasco Pasport). **b**, Picture of all components of the breath sampler for the non-monolithic impactor including the 2 silicon sieves in the centre which are assembled using an infrared microscope, O-rings to ensure air-tight packaging, and an aluminium casing mounted with screws to ensure temperature stability during operation. **c**, In order to avoid condensation on top of the silicon sieves, the

breath samplers are heated until 70°C degrees in an oven. After heating, it takes more than 40' to cool down until dew point, ensuring a safe window for sample collection. **d**, Picture of the breath sampler for the monolithic sieve. **e**, Picture of all components of the breath sampler for the monolithic chip. As only 1 chip is used, assembly is far easier and less components are needed. **f**, Picture of the chip mounted in the aluminium casing inside the PMMA housing. **g**, Pictures describing the chip filling and clamping steps after sample collection. From left to right, the silicon chip is taken out of its housing with a plastic sterile tweezer and a RT-qPCR mix with detergent for lysis is added on top of the sieve for it to fill by capillary flow. After filling, the sieve is placed in the bottom holder on a Li2000A thermal tape laminated on silicon. A pre-cut silicone sheet is carefully placed on top and 20ul extra RT-qPCR mix is added in between. Finally, the clamp is closed by screws using a torque screwdriver set at 4cNm. **h**, CAD drawing of the bottom and top view of the PMMA clamp to seal the monolithic sieve together with the cross section of the final stack mounted in the custom thermal cycler.

Extended Data Fig. 5: Thermal cycler and data analysis for monolithic impactor

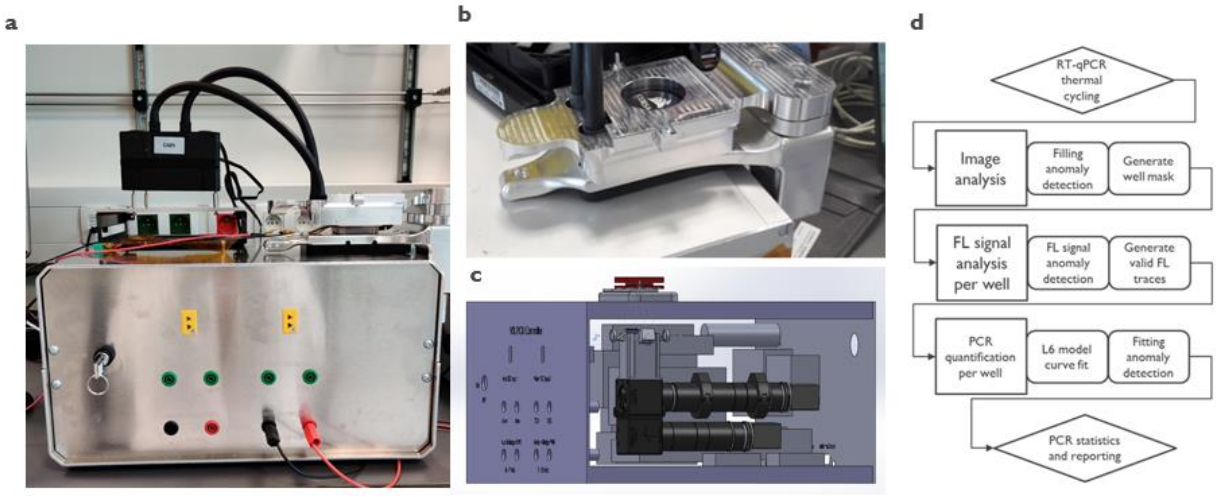

a, Picture of the custom-made RT-qPCR thermal cycler (front view). The instrument is connected to a PC (not shown) running a GUI for control of the hardware settings. **b**, Top image of the clamped sieve mounted on the shown thermal module; the thermal, metallic block performs rapid thermal cycling. **c**, CAD model of the optical module shown through an opened side panel. An inverted microscope is designed to acquire fluorescence images in sync with thermal cycling during RT-qPCR as illustrated in Fig. 4b-c. **d**, Schematic overview of the post-processing pipeline with key steps indicated. Acquired images are processed to generate an individual RT-qPCR curve per nozzle. Statistics of all curves generate the final PCR report with mean and average Ct values.

Extended Data Fig. 6: Percentage positive agreement between the nasopharyngeal swab and breath test for the different subjects per day during the longitudinal study.

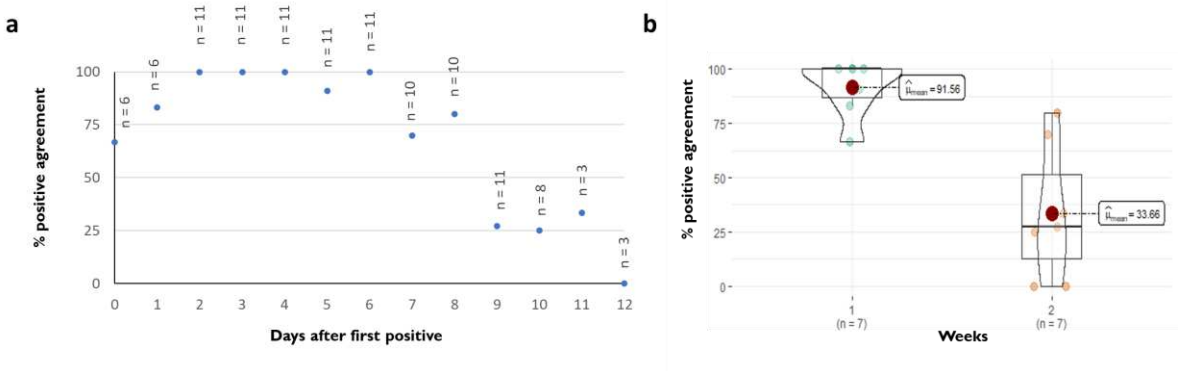

a, Overview of the percentage positive agreement per day of breath tests versus nasopharyngeal swab tests for the subjects included in the longitudinal study. Day 0 is marked as the day a first test turns positive. At day 0, two nasopharyngeal tests are positive while breath tests are negative; similarly, two breath tests are positive while the nasopharyngeal tests are negative. For 4 subjects, both tests are positive at day 0. The number of subjects included (n) to calculate the % positive agreement are indicated with the maximum being 11 (i.e. the number of subjects included in the longitudinal study). **b**, Visualization of the difference in percentage positive agreement across weeks by means of combined box-violin plots. The green dots represent percentages of day 0 through 6; the pink dots represent percentages of day 7 through 13. The red dots represent the weekly average percentage. Percentages in week 1 (mean 91.56) were higher than those in week 2 (mean 33.66), t_{Welch} (7.94) = 4.54, p = 0.002, $\hat{g}_{Hedges}$ = 2.19, $CI_{95\%}$ [0.74, 3.58], n_{obs} = 14.

Extended Data Fig. 7: Schematic overview of the inclusion flow chart for the longitudinal study

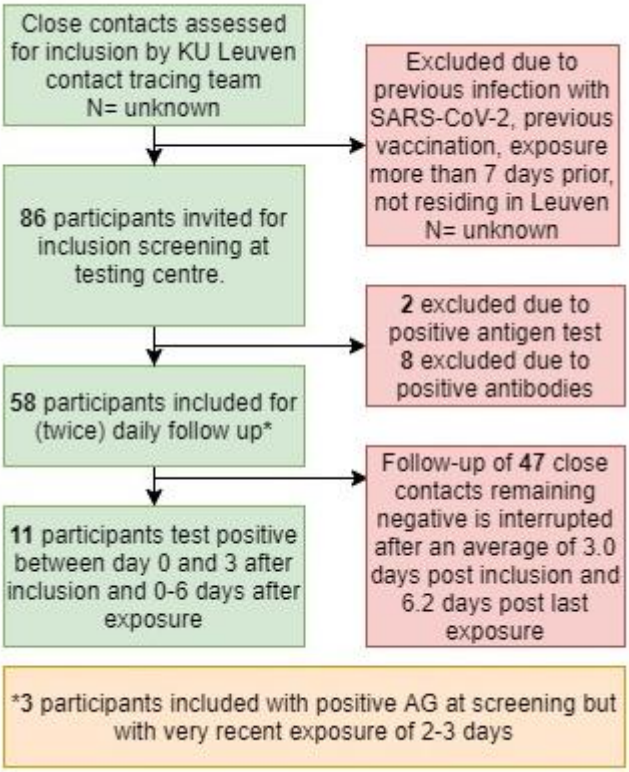

Schematic overview of the inclusion flow chart for the longitudinal study. Recent close contacts of confirmed COVID-19 positive cases were invited for inclusion if they had not previously been vaccinated or diagnosed with COVID-19, were able to attend the testing center and provide informed consent and planned to reside in the Leuven region during quarantine. A total of 86 suitable subjects underwent screening tests for inclusion (1 to 6 days after last exposure, mean = 3.1 days): rapid antigen (AG) testing on nasopharyngeal swab, RT-qPCR testing on breath, saliva and nasopharyngeal (NP) swab and blood antibody testing. 2 were excluded following a positive antigen-tests in combination with a history suggestive of late-stage infection. 8 were excluded following a positive antibody test. 3 were included despite testing positive on all diagnostics tests on day one since their assessment of symptoms and exposure history suggested likely recent infection. 58 subjects were followed up daily for 5 to 7 days after exposure. A total of 11 tested positive during follow up (0 to 3 days after inclusion, mean = 0.6 days). All but one had a negative RT-qPCR test in the 3 days prior to inclusion. They were followed up for 7 to 18 days (average 11.5). The first 6 subjects were sampled twice daily for saliva

and breath RT-qPCR and once daily for nasopharyngeal RT-qPCR and antigen test. Intermediate data analysis revealed limited variation in same day Ct values, prompting a switch to once daily sampling of subjects for all diagnostic tests.

SOURCE DATA

Source data 1: results of clinical trial 1 (breath tests in hospitalized patients)

Source data 2: results of clinical trial 2 (comparison of breathing methods)

Source data 3: results of clinical trial 3 (longitudinal data)